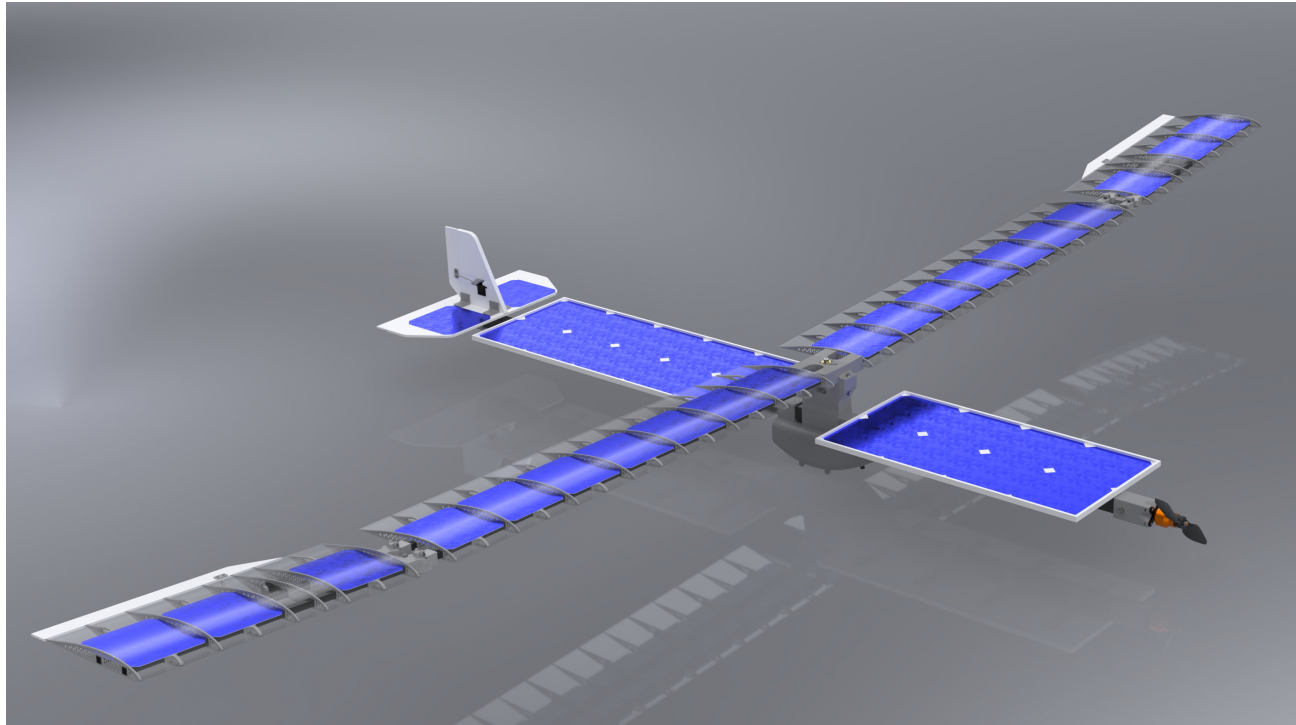


SPMA Ranger

Ethan Matzner, Fabio Nunez Del Prado, Emiliano Villicana Brugada,
Jorge Armando Ramos, Jayden Kevin Micah Dore, George Hawkins III



The authors are with the Department of Mechanical Engineering, Columbia University, New York, NY (eam2296, fan2112, ev2492, jar2359, jkd2147, geh2133 [@columbia.edu]). This material is based upon work developed in the MECE E3420 / E3430 Engineering Design Courses

Abstract—The SPMA Ranger is an autonomous, solar-powered, and modular glider employed to promote wildlife conservation against poaching. It is equipped with an onboard thermal camera and machine learning system to fly autonomously, detect unauthorized human presence, and provide real-time GPS alerts. Its renewable power system and modular design makes it a low-cost, sustainable, and simple-to-deploy solution for rangers working across large protected areas.

I. INTRODUCTION

Wildlife poaching continues to be one of the most critical conservation issues on the planet. Although there is progress in some areas, poaching continues to threaten many animals, with over 400 rhinos and nearly 20,000 elephants poached annually for their tusks and horns [1]. The threat even extends to the rangers, with over 150 being killed annually worldwide [2].

Current anti-poaching technology—like GPS collars, anti-snare equipment, and embedded chips—is typically reactive, intrusive, or useless at preventing harm [3] [4] [5].

To better meet this, we created the Solar-Powered Modular Aerial Ranger (SPMA Ranger), an autonomous UAV to assist rangers through proactive human detection. It employs a thermal sensor and GPS telemetry to autonomously surveil reserves and alert ground crews to intrusions prior to damage. Its solar-powered, modular design allows for long flight times, easy deployment, and inexpensive fixes (Fig. 1).

SPMA Ranger is constructed employing light carbon fiber rods and 3D-printed PLA components to provide strength and modularity. Power supply provides stable 12V and 8A with the use of 40 solar panels in two series parallel strings. The initial series of flight testing suggested roll instability at low speed, which was addressed through inclusion of inboard ailerons.

We followed FAA CFR safety guidelines and ASTM F2910 and AIAA's Design/Build/Fly guidelines [6] [7] [8]. Onboard thermal classification is achieved with a machine learning model on a Raspberry Pi. This is intended to classify human vs. animal in real time with low false positives.

The SPMA Ranger provides a scalable, sustainable, and deployable solution to conservation with emphasis on autonomy, modularity, and use of renewable energy for field deployment.



Fig. 1: Completed SPMA Ranger Prototype.

II. METHODS

A. Design Constraint 1: Dimensions and Sizing

The primary constraints that dictated the design of the SPMA Ranger were the brushless motor needed and the solar panels selected. These choices had cascading effects that determined the wing sizing, tail sizing, and much more.

In the electric UAV world, brushless motors are generally tied to a compatible operating voltage or voltage range determined by the LiPo battery size they are made to be used with. LiPo batteries are primarily grouped by their voltage, which is a function of the number of individual cells. Each cell operates between 4.2V and 3.7V, depending on its charge level.

After researching what solar panels other UAVs had used there was a clear preference for Sunpower Flexible Solar Cells [9]. The panels are lightweight, efficient, and relatively inexpensive, with a cost per panel of less than \$4.50 for a 3.6 W panel. Taking the power output of the panels listed on the website [10] as 0.6 V and 6 A, the panels need to be in series groups of 6 or 7 to represent each battery cell in terms of voltage. Looking at the same prior art as before, previous attempts at solar-powered UAVs have varied between using 3 or 4-cell compatible motors. The attempts that used 4-cell compatible designs tended to be bulkier and less efficiently built, so it was determined that if weight reduction was prioritized, a 3-cell compatible design would be feasible. This meant that 20 panels would be needed to mimic the voltage of 3 cells; using this assumption, 20-panel units could be added to scale the amperage.

Reviewing a brushless motor sizing and power guide [11], indicated that a motor with a maximum continuous draw of 10 A could produce up to 2 lbs of thrust. This meant that 40 panels could sufficiently power the motor and have excess power to charge the battery during flight. After purchasing this motor, these current draw assumptions were tested, and at the maximum throttle, the motor drew approximately 10 A.

Using the assumed motor thrust, calculation then began on the approximate mass that the aircraft could take off with. After reading several forums and guides on remote-controlled (RC) glider thrust-to-weight ratios, 0.3 was generally found to be the agreed-upon number [12]. This meant that the mass of the aircraft could be up to 6.67 lbs (2 lbs / 0.3).

Based on the available materials in Mudd, a square carbon fiber tube 1 inch wide and 5 feet long was selected as the central structural component of the SPMA Ranger. This rod was selected for its high strength and low weight. The rod was under 0.1 lbs/foot and could easily hold 34 lbs in testing, simulating 5 Gs in the heaviest configuration of the Ranger based on the selected motor. With a length of 5 feet, the rod had space for approximately 20 panels, in two rows of 10 (when including the additional 2 panels mounted on the tail). This meant that the wing would need to house the remaining 20 panels.

For the wings, an airfoil shape needed to be chosen before the design of solar panel mounts could be considered. Airfoil selection for a glider generally prioritizes maximizing lift at low speeds, while also aiming to minimize drag where possible. Considerations were also made regarding the principle that monokotting (a light-weight method of constructing wings for RC aircraft, wherein a skeleton is wrapped in a plastic film creating a firm outer skin) cannot be used to make concave shapes. This left a few very similar airfoils, but the s7055-il was selected for its softer curves as seen in Figure 2, which would make manufacturing easier.

With the constraint of 20 panels needing to go in the wings, the chord length would need to be at least 5 inches. A 5 inch chord would not leave sufficient space for a structural rod to run through the wing as well, so the chord was increased to accommodate the rods. To size these carbon fiber rods, very simple tests were performed using scrap segments of small carbon fiber rods that were taken from the Columbia University Airplane Club (CUAP) storage area. A rough approximation of the loads expected went as follows: 20 panels x 5 in. = 8.33 ft. 8.33 ft x 1.5 factor of safety = 12.5 ft. This wingspan could then be divided in half to simulate the load on each of the rods used. The maximum mass of 6.67 lb was then considered to be applying a downward force at one end of the rod, and the lift would be a point load at the opposite end. This method can be used to approximate a 2.5 G load on a set of wings [8]. Applying the calculated torque to each of the rod samples found led to all of the small rods failing; however, by using 2 rods or halving the torque, the 0.4 in. rod sample was the smallest sample that could withstand the expected loads.

With the 0.4 in. cross section needing to fit under the 5-inch wide area of the solar panel, the airfoil needed a chord of at least 8.4 in. Research on RC gliders and full-scale gliders indicated a range of aspect ratios from about 6:1 to 15:1. Based on the calculations for the minimum chord, a wingspan of up to 10.5 ft would be within the acceptable range. Seeing that RC gliders tended in the direction of the lower bound of aspect ratios, the wing was designed to be as small as possible while still holding the 20 solar panels needed. With the space needed for the hinge and the structural ribs, the wing was 10 ft long.

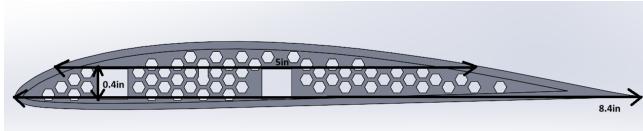


Fig. 2: Airfoil Dimensions

After manufacturing the wings and the majority of the other components, such as the motor mount, electronics compartment, fuselage solar panel mounts, and landing gear, everything was placed on the rod to calculate the weight and balance of the Ranger. Guides generally state that the center of lift should be 25-35% back from the front of the chord of the wing [13].

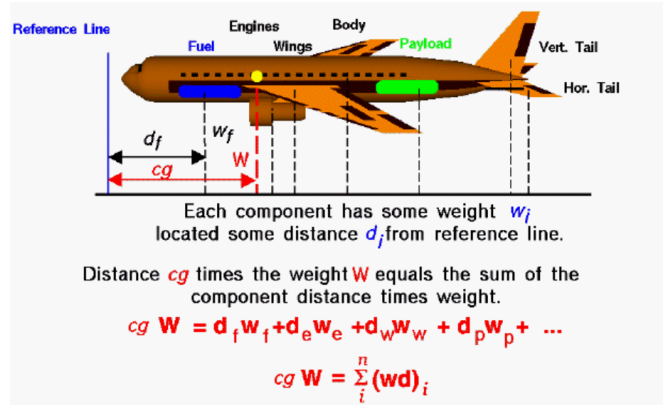


Fig. 3: Center of Gravity Diagram

This was then used to find an approximate wing position so that calculations could be made to find the approximate tail size. The equations for sizing vertical and horizontal stabilizers are, respectively:

$$C_{VT} = \frac{S_{VT} \cdot L_{VT}}{S_W \cdot b} \quad (1)$$

$$C_{HT} = \frac{S_{HT} \cdot L_{HT}}{S_W \cdot c_{MAC}} \quad (2)$$

Where C_{VT} and C_{HT} are the dimensionless variables that relate the relative size of the wing to the size of the vertical and horizontal stabilizers, respectively. S_{VT} and S_{HT} represent the areas of each stabilizer, L_{VT} and L_{HT} represent the distance from the aerodynamic centers of the wing and stabilizers, S_W is the area of the wing, c_{MAC} is the mean aerodynamic chord, and b is the wingspan.

The documentation used for the volume ratios comes from a design guide for full-sized aircraft [14], but it was assumed that the ratios would scale to this smaller-sized aircraft, since RC models frequently copy the shape of full-scale aircraft. The values for the sailplane type aircraft were selected because they are closest to the Ranger aircraft style, so $C_{VT} = 0.02$ and $C_{HT} = 0.5$ were used.

From these equations, it was concluded that based on the above ratios in the table consulted, a wing area of 1008 in², a mean aerodynamic chord of 8.4 in. from above, L_{VT} and L_{HT} values of 36 in. Based on weight and balance tests, the stabilizer areas should be approximately 67.2 in² and 117.6 in² for the vertical and horizontal stabilizers, respectively.

The horizontal stabilizer (H-stab) is intended to have room to mount two solar panels, giving a reasonable minimum width of approximately 11 in. when considering the additional width needed to mount the vertical stabilizer (V-stab). From there, the necessary length of the stabilizers could be calculated, and for the simplicity of construction, the same length was used for both stabilizers. This meant that the horizontal stabilizer should be 11 in. wide and 10.7 in. long, and the vertical stabilizer could be a right triangle 10.7 in. long and 12.6 in. tall. After consulting the market of remote control gliders, some minor changes were made seeing as

the horizontal stabilizers were made more aerodynamic by switching from a rectangular to a more angular trapezoidal design that many gliders employ. This change shortened the horizontal stabilizer, meaning that the vertical stabilizer would need to be taller to have the same area, but the shape was changed from a right triangle to a trapezoid to maintain the same area without a dramatic height increase.

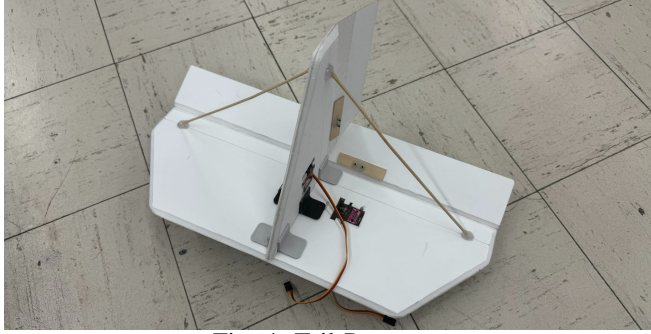


Fig. 4: Tail Prototype

B. Design Constraint 2: Structural Design

Our design process was molded by structural constraints stemming from expected loads during flight operation. Throughout this process, we conducted quantitative analyses, in the form of Finite Element Analysis (FEA) using SolidWorks software, on a set of parts: the outer wing hinge, the wing mount, and the motor mount.

A common methodology was employed for these analyses. Firstly, we calculated the expected loads on each part. Then, we defined the areas of fixture as well as the loading characteristics (magnitude, distribution, and direction) in a SolidWorks static study. After this, we would proceed to run multiple studies with increasing mesh densities, using solid tetrahedral elements. The results of these studies were then plotted against the total mesh elements in order to verify that there existed converging output. This step follows good practice in FEA study since the simulation accuracy depends on the mesh refinement, therefore when further mesh has negligible effect on the output we call it a trustworthy result. Note that we defined further meshing negligible once we reached a $\pm 5\%$ difference between successive studies. Finally, with our trusted results, we qualitatively analysed that the stress values seemed reasonable and that the factor of safety (FoS) matched or exceeded a value of 2.0 all throughout the part.

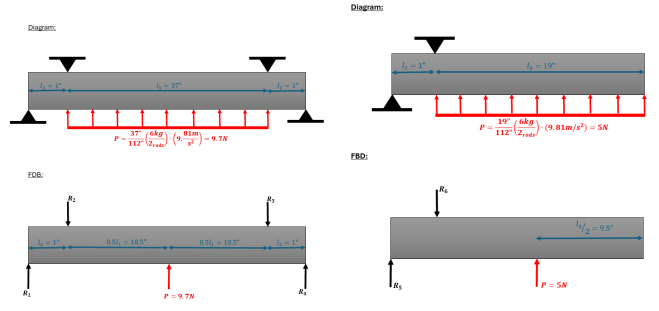
We based our desired value of FoS on the established standard mentioned in a publishing from NASA. The publishing outlines the development and evolution of FoS criteria in aerospace applications. Most standards mentioned in the publication dictate a FoS of 1.5 or 1.4, however a value of 2.0 is cited as used in some labs. Considering the fact that our plane is not designed to directly interact with live subjects, we considered the 2.0 FoS as a conservative benchmark for all our components. [15]

One last important detail from our FEA studies is that we had to define specific mechanical properties for our parts.

All three parts were manufactured from traditional PLA using Bambu Lab X1C and A1-Mini 3D printers. Since this manufacturing process results in an anisotropic workpiece, we had to conduct further investigation than simply finding PLA's pure mechanical properties. Our investigation resulted in the finding of a 2019 publication titled "Mechanical Properties of 3D-Printing PLA Parts Subjected to Bending Stress and Fatigue Testing". [16] With this study, we were able to properly define the mechanical properties unique to each part given the direction of load with respect to the plane of the print as well as the layer height and infill.

In continuation, we will define in more detail the load calculations as well as the fixture and load definition in SolidWorks for the outer wing hinge, wing mount, and motor mount.

1) Outer Wing Hinge: To calculate the expected load on the hinge, we began with an engineering idealization which, although not entirely realistic, gives a good idea of the loads to be expected. This idealization was to treat both wing segments, on either side of the hinge, as solid simply supported beams with supports located according to the shaft-to-hinge attachment. This analysis also idealized the load as an evenly distributed lift force perpendicular to the bottom surface and equal in magnitude to the plane's weight. This is founded in the fact that, during steady-state flight operation, the lift of a plane is equal in magnitude and opposite in direction to its weight. [17, p. 3][18] See figure 5 for the force diagrams and FBDs of this study.



(a) Inner Wing (b) Outer Wing
Fig. 5: Full Wing Force Diagram and FBD

Then to apply these loads to the hinge, we opted for a distributed load along the inner top and bottom faces of the hinge. This load was distributed decreasing linearly from the edge of the loading face towards the center of the shaft-to-hinge attachment pocket. This decision was founded on a multifaceted analysis process. Firstly, we understood that the shaft would behave like a lever with its pivot in the center of the pocket when under load due to lift. Then, due to the fact that the pocket has a tight fit around the wing shaft, not all the load would be concentrated at the edges and instead would logically taper off towards the pivot. We decided to idealize this as a linear relationship for the sake of simplicity. In the intent to justify our load distribution analysis, we could not find direct examples of this situation in literature, however we did find other similar engineering applications which concur with our analysis, such as a stress

analysis on a lug subjected to “single-shear joint” stress. [19]

The areas and definition of fixture were simpler to determine. We fixed all the inner surfaces of the screw locations which lock both halves of the hinge as well as the plane surfaces parallel to the head and nut.

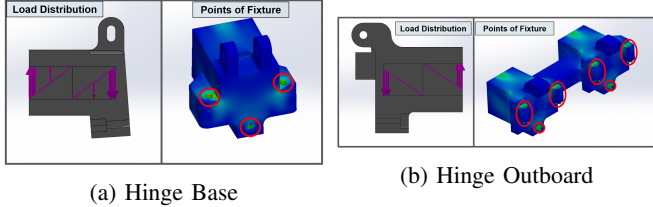


Fig. 6: Full Hinge Loading Distribution and Fixtures

2) *Wing Mount*: To calculate the expected load for the wing mount, we used the same approach as for the outer wing hinges. This meant that the four pockets experienced the same load as did the pockets of the inner half of the hinge. As for the areas of fixture, these were set at the inner surface of the three screw holes: the outer two intended for locking the rotation and the center pivot screw.

Images of the loading distribution and the areas of fixture are included in Appendix V-B.

3) *Motor Mount*: The plane’s motor was attached to the motor mount by four screws. Logically, we defined the loads as an even distribution among the four flat portions where the nuts of the screws push against the mount (see figure 15 in Appendix V-C). Furthermore, the magnitude of the loads were defined by the motor’s maximum thrust characteristics which are defined by the manufacturer as 0.9kg. This thrust was taken to be divided equally between the four mounting screws.

Then, the fixture of the part was defined as the two inner surfaces of the set screw holes.

Images of the loading distribution and the areas of fixture are included in Appendix V-C.

III. RESULTS

Based on the sizing constraints of the SPMA Ranger stemming from the solar panels and motor choices, the following decisions were made:

TABLE I: Sizing Constraints Summary

Parameter	Value	Parameter	Value
Solar Panel QTY	40 Panels	Fuselage Rod Width	1 in
Panel Voltage	0.6 V	Fuselage Rod Length	5 ft
Panel Current	6 A	Wing Rod Width	0.4 in
Panel Size	5×5 in	Wing Span	10 ft
Motor Power	120 W	Chord Length	8.4 in
Motor Thrust	1 lb	Wing Area	1008 in ²
Motor Current	10 A	Aspect Ratio	14.3 : 1
Thrust to Weight	0.3	H-Stab Area	117.6 in ²
Max UAV Weight	6.67 lb	V-Stab Area	67.2 in ²

TABLE II: Motor Mount Stress & Material Safety Summary

Parameter	Value	Unit
Applied Thrust Force	9.0	N
Material Yield Strength	50.0	MPa
Max von Mises Stress (FEA)	27.4	MPa
Max Displacement	0.42	mm
Safety Factor	10	–

With regards to our quantitative analysis for the plane’s structural constraints:

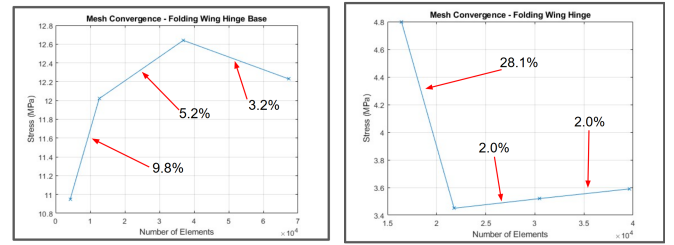
A. Outer Wing Hinge

From the beam analysis mentioned in the Methods section, we calculated the reaction forces which indicate the expected loads on the hinge. See table III for a summary of these values and Appendix V-A for a detailed derivation.

TABLE III: Wing Load Analysis

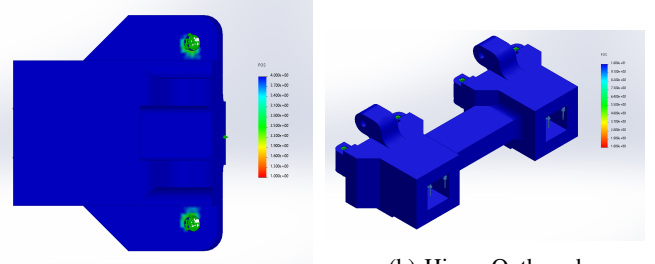
Reaction Force	Value (in Newtons)
R_1	89.91
R_2	94.77
R_3	94.77
R_4	89.91
R_5	47.50
R_6	52.50

After running the multiple studies and confirming a mesh convergence, illustrated in figure 7, we had confidence in our results and deemed them final.



(a) Hinge Base (b) Hinge Outboard
Fig. 7: Full Hinge Mesh Convergence

We then looked at the FoS plot for both halves of the hinge and observed that the entire part displayed a FoS of 2.0 or larger at any given point. See figure 8 for an image of the FoS.



(a) Hinge Base (b) Hinge Outboard
Fig. 8: Full Hinge FoS

B. Wing Mount

As mentioned in the Methods section, the loads we applied to the wing mount mimicked those applied to the inner half of the hinge. These are outlined as R_1 and R_2 in table III. Then, similar to the hinge, we again ran the study multiple times until mesh convergence was reached and then we extracted the values and plot for the FoS. These values demonstrated a FoS greater than 10.0 all throughout the part. (see figure 14 in Appendix V-B)

C. Motor Mount

From the load distribution mentioned in the Methods section, we found that the load applied at each of the four mounting screw sections totaled 2.2N per section. Having set this value and ran multiple studies to confirm mesh convergence, see figure 17 in Appendix V-C, we found that the FoS demonstrated a value larger than 10.0 all throughout the part (see figure 18 in Appendix V-C).

IV. DISCUSSION & CONCLUSION

The decisions that went into the sizing and solar panel layout of the SPMA Ranger were made using information from a wide variety of sources including YouTube videos from experienced UAV builders, UAV forums, research papers, and relevant articles. Compiling all this information required making a variety of compromises and assumptions some of which appear to have been reasonable and others which may have fallen short of expectations. The primary tool to test the assumptions made was a day of flight-testing performed with the first prototype of the SPMA Ranger. During testing, the aircraft successfully lifted off the ground and flew for several seconds before an issue with roll control caused the prototype to bank to the left and stall, causing a crash that broke the left wing hinge at the outer half of the hinge.

One of the biggest assumptions from the start was the choice to select a smaller 3-cell compatible motor, assuming that the aircraft could be made relatively light. This assumption proved very reasonable as the aircraft came in under 6.5 lb, which is over 0.17 lb lighter than expected. The motor choice was also validated during testing when the motor was able to get the SPMA Ranger prototype off the ground during a flight test. The carbon fiber spars were also selected on a variety of assumptions made regarding the loads of flight, and these assumptions appear to have been validated as the wings were strong enough to endure a simulated 2.5 Gs and even survived a significant crash of the Ranger prototype during testing. The general design of the wings, such as span and the chord were also validated when the Ranger lifted off the ground during flight testing. Another key assumption made regarded the scaling of the horizontal and vertical stabilizers and if the guide used for full sized aircraft would apply to much smaller UAVs. This assumption appears to have been reasonable as there was sufficient pitch and yaw stability during flight according to the pilot, demonstrating that the assumptions made were reasonable.

One key assumption that led to the aforementioned crash was the sizing of the control surfaces. The elevator and rudder appear to have been sufficiently sized as they were able to keep the Ranger straight during takeoff and were able to get the aircraft off the ground. The ailerons however, were insufficiently positioned and sized, as the pilot explained the cause of the crash was a lack of roll control. The calculations for all three control surfaces came from the same document that includes a guide on the relative sizing of these features [14]. Different guides gave different ways of calculating the

aileron sizes but something was likely calculated incorrectly or using an equation that did not scale properly to the size of the glider as some forums for RC airplanes generally explained an appropriate aileron size of 10 to 15% of the wing area but the formulas used produced ailerons that were just 7.5% the wing area.

Regarding the parts we studied for the structural stability of the plane:

A. Outer Wing Hinge

The most important detail from the hinge's study's results was the FoS. After analysing these, we corroborated that both halves of the hinge demonstrated a FoS of 2.0 or greater all throughout the hinge. Recalling from the Methods section, 2.0 is the minimum FoS that we were working with, therefore we deemed our part fit for the conditions we expected.

After flying the plane, we are confident in saying that the part does sustain the expected loads and does properly perform its function while also maintaining the structural integrity of the wing. Interesting to note, when the plane crashed during our testing, the outer section of the left wing broke off exactly at the hinge. Our part was not designed to sustain this style of impact, therefore we still consider the test a success and even find that it has an added benefit of localizing the failure point at this cheap and easy to replace part rather than at another area such as the body of the wing which would be more complicated and costly to fix.

B. Wing Mount

Similar to the hinge study, the most important detail from the wing mount's study was the FoS. As mentioned in the Methods section, this value came out greater than 10.0 throughout the entire part. From this, we determined the part to be entirely safe for our expected conditions, for which we were using a minimum FoS of 2.0.

When we tested the plane, the wing mount performed well and we did not notice any flaws in the design nor its structural soundness. From this test, we gained even more confidence that our FEA study was accurate.

C. Motor Mount

As mentioned for both other parts, the value we sought from this study was the FoS. Similar to the wing mount, the motor mount also displayed large FoS values exceeding 10.0 everywhere along the part. From this, again, we determined the part to be entirely safe for our expected conditions.

Similar to the wing mount, we noticed zero signs of weakness or structural instability with the mount and are therefore extremely confident in the accuracy of our FEA studies.

V. APPENDIX

A. Wing Load Analysis

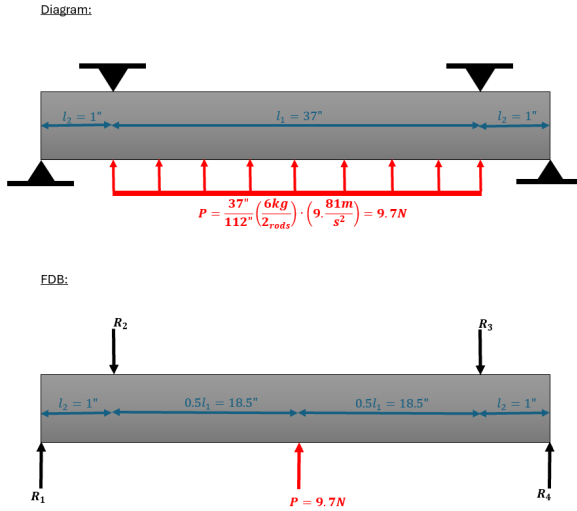


Fig. 9: Inner Wing Force Diagram and FBD

1) *Inner Wing Calculations*: As shown in the image with the diagram above, figure 9, the total lift force on each wing rod from the distributed load is 9.7 N

Then, applying static equilibrium equations:

$$\sum F_y = 0 \Rightarrow R_2 = R_1 + P \quad (3)$$

$$\sum M_{R_2} = 0 \Rightarrow R_1 = \frac{P \cdot l_1}{2 \cdot l_2} = \frac{(9.7 N) \cdot 37''}{2 \cdot 1''} = 179.82 N \quad (4)$$

Substituting back into Equation (3):

$$R_2 = 179.82 N + 9.7 N = 189.52 N \quad (5)$$

By symmetry of the hinge configuration, the real value of the reaction forces is halved and equal on both sides:

$$R_2 = R_3 = 94.77 N$$

$$R_1 = R_4 = 89.91 N$$

2) *Outer Wing Calculations*: As illustrated in figure 10, the distributed lift force is calculated as 5 N. Now when we apply a vertical force equilibrium:

$$\sum F_y = 0 \Rightarrow R_6 = R_5 + P \quad (6)$$

Now take moments about point R_6 :

$$\sum M_{R_6} = 0 \Rightarrow R_5 \cdot l_2 = P \cdot \frac{l_1}{2} \quad (7)$$

$$R_5 = \frac{P \cdot l_1}{2 \cdot l_2} = \frac{(5 N) \cdot 19''}{2 \cdot 1''} = 47.5 N \quad (8)$$

Diagram:

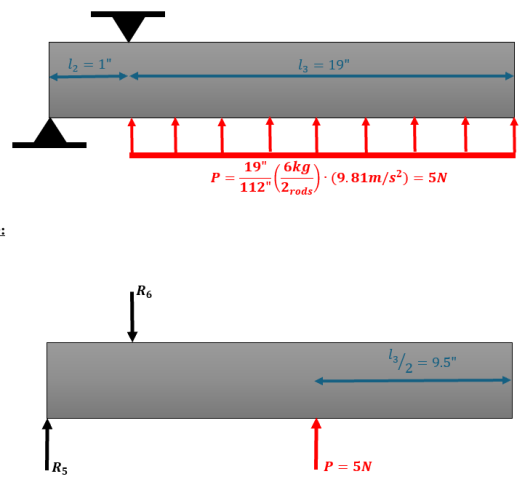


Fig. 10: Free-body diagram for second hinge section

And then substitute back into equation 6 and we get:

$$R_6 = 47.5 N + 5 N = 52.5 N \quad (9)$$

B. Wing Mount

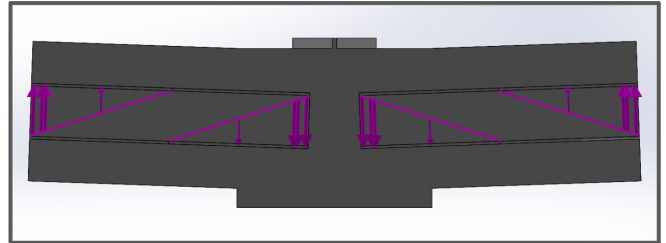


Fig. 11: Wing Mount Load Distribution

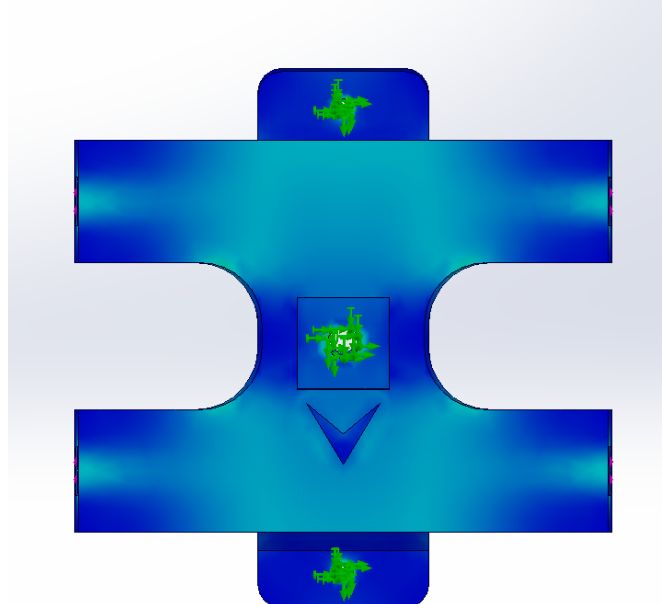


Fig. 12: Wing Mount Fixtures

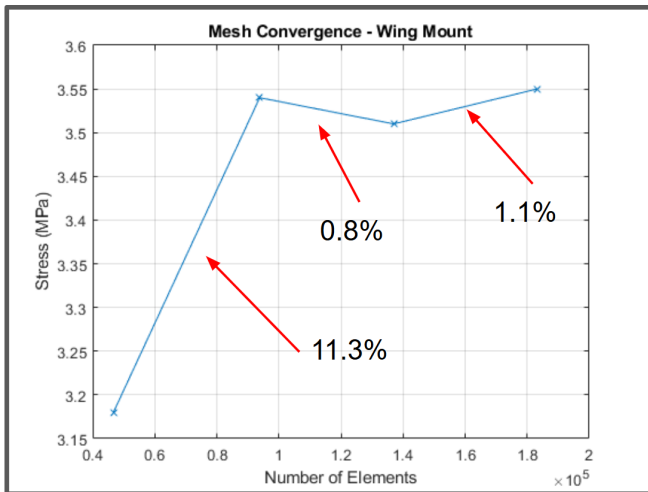


Fig. 13: Wing Mount Mesh Convergence

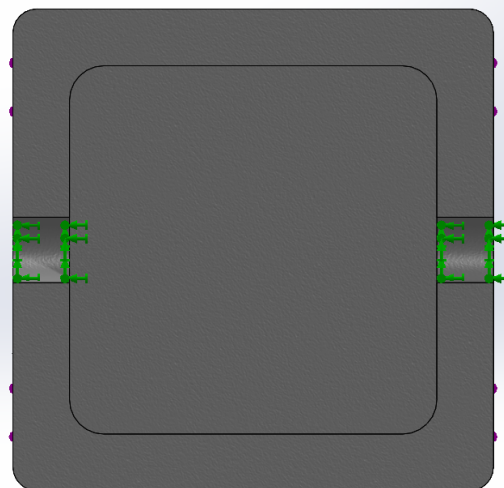


Fig. 16: Motor Mount Fixtures

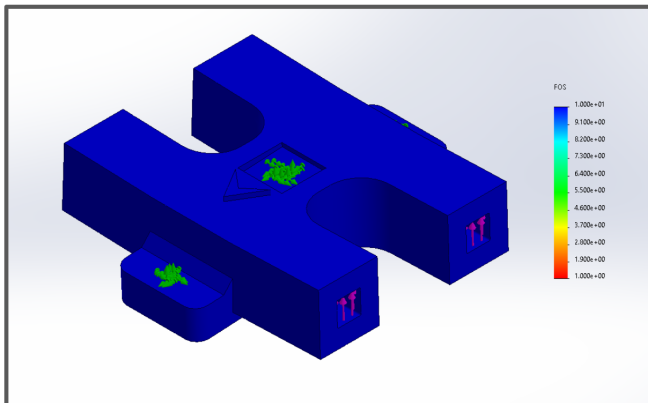


Fig. 14: Wing Mount Factor of Safety

C. Motor Mount

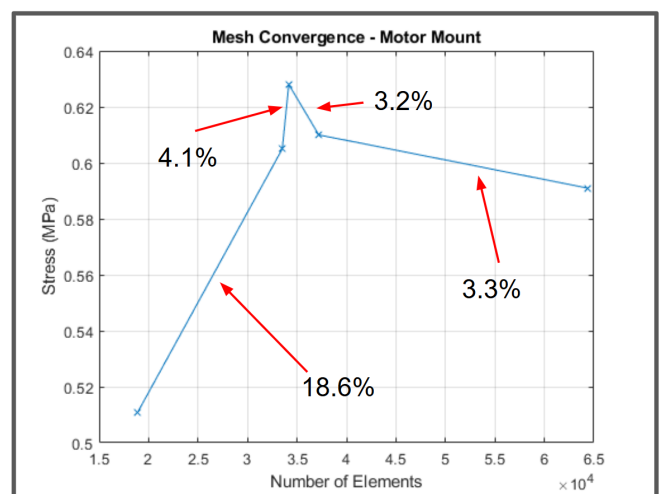


Fig. 17: Motor Mount Mesh Convergence

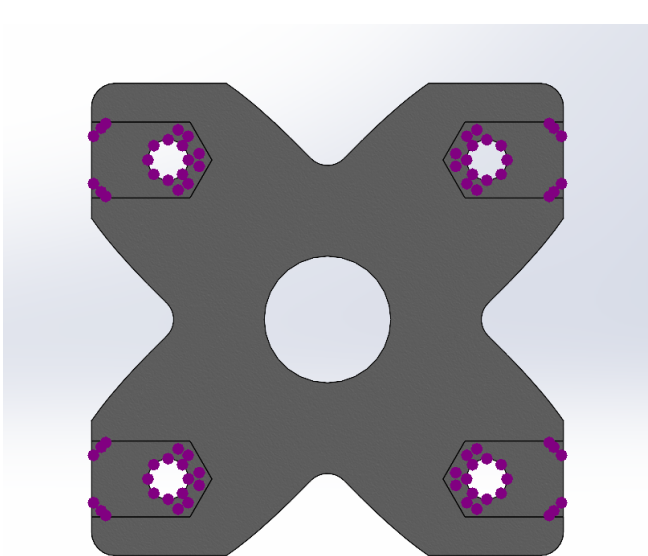


Fig. 15: Motor Mount Load Distribution

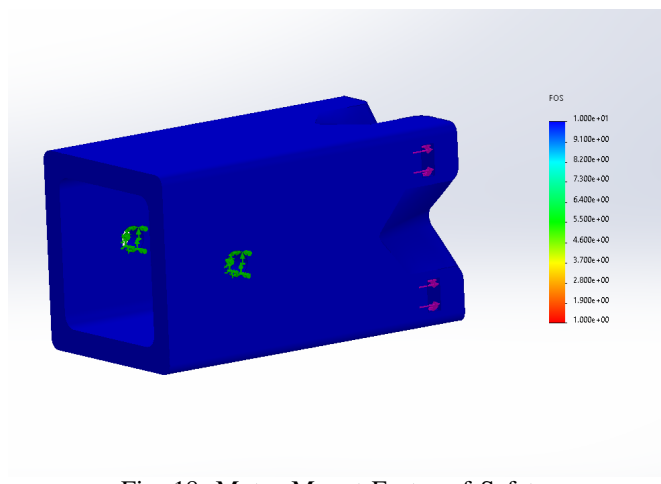


Fig. 18: Motor Mount Factor of Safety

REFERENCES

- [1] World Animal Foundation, "Poaching statistics & facts in 2024," *World Animal Foundation*, 2024. Accessed: 2025-05-11.
- [2] World Bank, "Risking lives to protect wildlife and wildlands: Stories from rangers in the field," *World Bank*, 2020. Accessed: 2025-05-11.
- [3] J. Doe and J. Smith, "Evaluating the effectiveness of anti-snare collars in reducing wildlife poaching," *Biological Conservation*, vol. 275, pp. 109–117, 2023. Accessed: 2025-05-11.
- [4] Montana Fish, Wildlife & Parks, "Limitations of tracking data," 2025. Accessed: 2025-05-11.
- [5] A. Smith and R. Johnson, "Poaching detection technologies—a survey," *Sensors*, vol. 18, no. 5, p. 1474, 2018. Accessed: 2025-05-11.
- [6] Federal Aviation Administration, "Small unmanned aircraft systems (uas) regulations (part 107)," 2025. Accessed: 2025-05-11.
- [7] ASTM International, "Astm f2910-22: Standard specification for design and construction of a small unmanned aircraft system (suas)," 2022. Accessed: 2025-05-11.
- [8] American Institute of Aeronautics and Astronautics, "Aiaa design/build/fly competition," 2025. Accessed: 2025-05-11.
- [9] James Whomsley, "How to build a solar powered rc plane," October 2024.
- [10] SunPower, "Sunpower flexible solar cells e60 c60 5x5 3.6w monocrystalline cells for diy panels."
- [11] Flashhobby, "Out-runner brushless motor flashhobby 2212."
- [12] JoyPlanes, "How to choose the right motor and propeller for your rc aircraft," 2020.
- [13] Tom Benson, "Center of gravity aircraft application." Accessed: 2025-05-11.
- [14] Andrew Wood, "Aircraft horizontal and vertical tail design," 2022.
- [15] C. T. Modlin, "The 1.5 1.4 ultimate factors of safety for aircraft spacecraft – history, definition and applications," 2014.
- [16] J. Antonio Travieso-Rodriguez, "Mechanical properties of 3d-printing polylactic acid parts subjected to bending stress and fatigue testing," 2019.
- [17] Mark D. Guynn, "Effective l/d: A theoretical approach to the measurement of aero-structural efficiency in aircraft design," 2015.
- [18] Greg Ciurpita, "Bending-moments," 2002.
- [19] Engineering Library, "Lug analysis," 2025.